PHYSICAL REVIEW B VOLUME 44, NUMBER 16 15 OCTOBER 1991-II

Optical properties of WSi_2

V.N. Antonov, Vl.N. Antonov, O. Jepsen, and O.K. Andersen
Max-Planck-Institut für Festkörperforschung, Stuttgart 80, Federal Republic of Germany

A. Borghesi, C. Bosio, F. Marabelli, and A. Piaggi
Dipartimento di Fisica "A. Volta," Università degli Studi di Pavia, Via Bassi 6, I-27100 Pavia, Italy

G. Guizzetti and F. Nava
Dipartimento di Fisica, Università degli Studi di Modena, Via Campi 213/A, I-41100 Modena, Italy
(Received 19 April 1991)

The optical properties of WSi_2 single crystal were investigated between 0.01 and 23 eV. The near-normal-polarized reflectivity was Kramers-Kronig analyzed to determine the dielectric functions over the whole spectral range. Some constraints were imposed in order that the resulting spectra fit those directly measured by ellipsometry in the energy range from 1.4 to 4.9 eV. The optical response of polycrystalline films of WSi_2 was also analyzed. Some differences between the single crystal and the thin-film optical functions are underlined, particularly near 0.5 eV, where a low-absorption region exists. Moreover, the electronic states and the optical properties of WSi_2 were calculated within the local-density approximation using the semirelativistic linear-muffin-tin-orbital method. The band structures, the ℓ-projected densities of states, the complex dielectric function, the optical conductivity, the optical reflectivity, and the electron energy-loss spectrum were evaluated in the energy range from 0 to 10 eV. The agreement with the experimental data is good.

I. INTRODUCTION

Refractory metal silicides have a growing interest in the very large scale integrated technology as materials for gate electrodes and interconnections. Tungsten disilicide is particularly studied due to its high conductivity and to its capability of forming a passivating SiO_2 layer.[1,2] Up to now, most of the investigations have been devoted to the deposition process, the annealing procedure, the composition, and the structure, as well as to the electrical transport properties.[2–5] The optical response of WSi_2 as single crystal has been analyzed by ellipsometry in the energy range from 1.3 to 5 eV and by reflectometry from 0.6 to 3 eV by Ferrieu *et al.*;[6] the transmittance of WSi_2 polycrystalline films in the far-infared region is presented in Ref. 7, where a discussion on the vibrational modes is given. Nevertheless, a more exhaustive work on the optical properties does not exist at present. As the theoretical analysis is concerned, Battacharyya, Bylander, and Kleinman[8] have carried out fully relativistic band calculations for WSi_2, using norm-conserving pseudopotentials. They reported the band structures, the decomposed partial densities of states, and the cohesive energies. On the other hand, Itoh[9,10] investigated the Fermi surface of tungsten disilicide by means of a self-consistent semirelativistic band-structure calculation, performed with the linear–muffin-tin-orbital in the atomic-sphere approximation (LMTO-ASA) method using the von Barth–Hedin[11] exchange-correlation potential. Nevertheless, as far as we know, no theoretical investigations of the optical properties has been published up to now.

It is very interesting then to study this disilicide optically over a more extended range, to compare the single-crystal properties with those of the thin film and to correlate the experimental optical spectra with the theoretical ones.

We report in this paper a wide optical characterization of WSi_2 from the far-infrared (0.01 eV) to the vacuum ultraviolet (23 eV). Reflection and spectroscopic ellipsometric measurements are presented. A low absorption coefficient region exists near 0.5 eV, and some interesting differences in this spectral region between the single-crystal and the thin-film optical functions are shown and discussed. Care is devoted to the determination of the complex refractive index of WSi_2 as polycrystalline film. This is important in view of the accurate measurement of the thickness of the oxide grown on the silicide, generally performed by fixed wavelength ellipsometers.

We also present the calculated optical spectra of WSi_2 in the energy range from 0 to 10 eV as obtained from the electronic energy bands and wave functions using the local approximation to the density-functional theory (LDA).[11] Although the LDA aims to describe ground-state properties, we shall use it for the electronic excitations, first of all because this is presently the only *ab initio* approach for *d*-band metals and their compounds, and because past experience indicates that its results are accurate within about 1 eV for metals with broad bands.

 ©1991 The American Physical Society

II. EXPERIMENTAL AND COMPUTATIONAL DETAILS

A. Experiment

WSi_2 single crystal was grown by the Czochralski technique. The crystal was pulled from rf-levitated melt in a modified Hukin-type crucible by direct melting of metal rods (with purity of 99.99%), high-purity (99.9999%) silicon lumps, and subsequent quenching. The details of the process are reported elsewhere.[12] The single-crystal rods were then mounted on a goniometer and oriented using the x-ray Laue diffraction (XRD) technique.

WSi_2 thin films were prepared by simultaneous evaporation of high-purity metal and silicon in a dual electron-beam evaporation system. Typical deposition rates were 0.5 nm/s for the metal and 1.2 nm/s for silicon. The pressure in the evaporation chamber was 1×10^{-8} Torr. The films were deposited at room temperature on 120-nm-thick thermally oxidized Czochralski silicon, in order to make electrical transport measurements too.

The samples were heated at 900 °C for 30 min in a flowing helium tube furnace where the helium was purified passing through a bed of titanium held at 1000 ° C. In order to reduce the intake of impurities upon thermal annealing, attention was taken by covering the thin films surface with another silicon wafer.

Rutherford backscattering spectroscopy (RBS) with a 2-MeV $^4He^+$ ion beam was used for depth composition analysis and for determining the film thickness (with an uncertainty of ±10 nm). XRD allowed the identification of the silicide phases present in the films. A Bragg-Brentano reflection goniometer with scintillation counter employing Cu $K\alpha$ radiation was employed. The XRD spectra indicated that after the thermal treatment no metal-rich silicide or hexagonal WSi_2 are present, but only tetragonal WSi_2 and unreacted silicon. Finally, Auger-electron spectroscopy showed that the oxygen and carbon levels in the films were below the detection limit (0.1%).

Near-normal incidence reflection measurements at room temperature were performed in the energy range from 0.01 to 0.5 eV by a Fourier transform spectrometer Bruker IFS 113v, with instrumental resolution of 0.5 meV and with a gold mirror as reference. In the case of WSi_2 single crystal, light was polarized by KRS5 and polyethylene grid polarizers in the medium-infrared (MIR) and in the far-infrared region (FIR), respectively. Moreover, due to the small dimensions of the sample ($5\times1\times0.5$ mm^3), we used a Bruker microscope and a homemade reflection accessory in the MIR and in the FIR, respectively.

Above 0.5 up to 6 eV we measured the WSi_2 film unpolarized reflectance with a Perkin Elmer 330 spectrophotometer. An Al mirror, whose absolute reflectivity was previously measured, was used as reference. The polarized reflectivity of WSi_2 single crystal was taken from 0.5 to 4 eV by a home-built prism spectrometer with a Zeiss double monochromator, more suitable to examine small samples. Light was polarized by a polarizing beam splitter. In this spectrometer an optical system equipped with a turning light guide allowed us to measure directly and alternatively the intensity of the focused incident and of the reflected light beam, so that we avoided reference mirrors.

Finally, near-normal absolute reflectivity measurements with polarized light were performed from 4.0 to 25 eV at the synchrotron-radiation facility BESSY in Berlin. A 2-m Seya-Namioka concave grating spectrometer was used. Reflected light was first converted from medium ultraviolet into near ultraviolet using sodium salicylate and then detected by an S20 photomultiplier. Spectra between 4.0 and 6.5 eV were taken with an MgF_2 window between the spectrometer and the sample chamber, while for spectra between 6.0 and 10.0 eV a LiF window was used. The spectra had to be corrected for stray light whose contribution is strong at the highest energies.

We want to point out that, in the overlapping spectral regions, the reflectivity values obtained by different spectrometers agreed within the limits of experimental uncertainty.

Ellipsometric spectra in the energy range from 1.4 to 4.9 eV were taken with a Sopra ellipsometer model ES4G.

B. Computational details

WSi_2 crystallizes in the body-centered tetragonal (bct) structure with six atoms per unit cell. The bct crystal structure of WSi_2 is shown in Fig. 1. The lattice constants are a=6.0698 Å, and c=14.806 Å,[13] with c/a= 2.439. The space group is $I4/mmm$. The corresponding Brillouin zone (BZ) is also shown in Fig. 1, where the symmetry points and lines are labeled in accordance with the standard of Ref. 14.

A detailed description of the LMTO-ASA method, including its use for compounds, is given elsewere.[15,16] The present calculations were carried out semirelativistically and with basis functions including angular momenta up to l=3 for tungsten and l=2 for silicon. The "frozen-core" approximation was adopted and the core charge distributions were evaluated from the solutions of the Dirac equation for free atoms.

Exchange and correlation contributions to both the atomic and the crystalline potential have been included through the density-functional description in the LDA of von Barth and Hedin.[11] The **k**-integrated functions have been evaluated by the tetrahedron method[17] on a grid of 189 **k** points in the irreducible part of the Brillouin zone, which corresponds to 3024 **k** points throughout the BZ.

The linear response of a system due to an external electromagnetic field with small wave vector is determined by the imaginary part $\epsilon_2(\omega)$ of the complex dielectric function $\tilde{\epsilon}(\omega) = \epsilon_1(\omega) + i\epsilon_2(\omega)$. We have calculated the dielectric function for frequencies well above those of the phonons and therefore we considered only electronic excitations. For these we used the random-phase approximation, neglecting local-field and finite life-time effects.[18] Moreover, due to the tetragonal structure of WSi_2, the dielectric function is a tensor. By an appropriate choice of the principal axes we could diagonalize it and restrict our considerations to the diagonal matrix elements $\tilde{\epsilon}^{\nu\nu}(\omega)$, with $\nu = x, y, z$. The interband contribution to $\epsilon_2(\omega)$ is given by

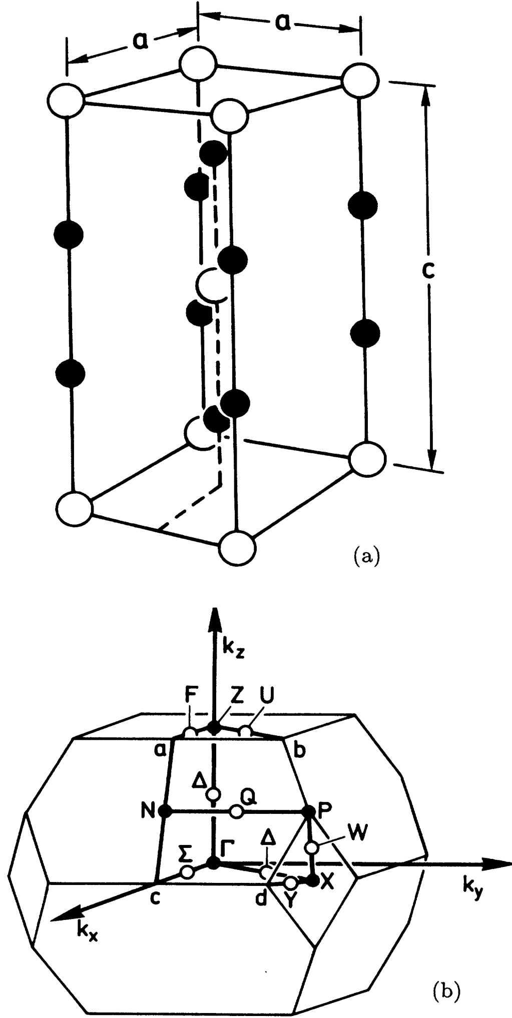

FIG. 1. (a) Body-centered tetragonal unit cell of WSi_2. Open circles correspond to tungsten atoms, filled circles correspond to silicon atoms. (b) Brillouin zone corresponding to the body-centered tetragonal structure ($c > a$).

$$\epsilon_2^{\nu\nu}(\omega) = \frac{8\pi^2 e^2}{m^2\omega^2} \times \sum_{n\neq n'}^{\text{unocc}} \sum_{n'}^{\text{occ}} \int_{\text{BZ}} |P_{nn'}^{\nu}(\mathbf{k})|^2 \delta(E_n^{\mathbf{k}} - E_{n'}^{\mathbf{k}} - \hbar\omega) \times \frac{d^3k}{(2\pi)^3}, \quad (1)$$

where $P_{nn'}^{\nu}(\mathbf{k})$ is the projection of the momentum matrix elements $\mathbf{P}_{nn'}(\mathbf{k})$ along the ν direction of the electric field $\mathbf{E}$. $E_n^{\mathbf{k}}$ are the one-electron energies.

After having evaluated (1) we calculated the interband contribution to the real part of dielectric function $\epsilon_1(\omega)$ from the Kramers-Kronig (KK) relation:

$$\epsilon_1(\omega) = 1 + \frac{2}{\pi} \mathrm{P} \int_0^{\infty} \frac{\epsilon_2(\omega')\omega' d\omega'}{\omega'^2 - \omega^2}, \quad (2)$$

where P stands for principal value. Finally, we obtained the total complex dielectric function by adding the intraband contribution. We neglected this contribution to $\epsilon_2(\omega)$ according to the perfect crystal approximation, since the defects and lattice oscillations are absent. On the contrary, the intraband contribution to $\epsilon_1(\omega)$ is given by

$$\epsilon_1^{\nu\nu}(\omega)|_{\text{intra}} = 1 - \frac{(\omega_p^{\nu\nu})^2}{\omega^2}, \quad (3)$$

where the squared plasma frequency is given by

$$(\omega_p^{\nu\nu})^2 = \left(\frac{e}{\pi\hbar}\right)^2 \sum_n \int_{\text{BZ}} \left(\frac{\partial E_n^{\mathbf{k}}}{\partial k^{\nu}}\right)^2 \delta(E_n^{\mathbf{k}} - E_F) d^3k. \quad (4)$$

We also calculated the optical conductivity $\sigma(\omega)$, the reflectivity $R(\omega)$, and the electron energy-loss spectrum $L(\omega)$ using the relations (1)–(4) and the following expressions:

$$\sigma(\omega) = \frac{\omega}{4\pi}\epsilon_2(\omega), \quad (5)$$

$$R(\omega) = \left|\frac{\sqrt{\tilde{\epsilon}(\omega)} - 1}{\sqrt{\tilde{\epsilon}(\omega)} + 1}\right|^2, \quad (6)$$

$$L(\omega) = \mathrm{Im}\left(\frac{-1}{\tilde{\epsilon}(\omega)}\right) = \frac{\epsilon_2(\omega)}{\epsilon_1^2(\omega) + \epsilon_2^2(\omega)}. \quad (7)$$

III. RESULTS

A. Optical response of WSi_2 single crystal

The reflectivities R for the incident electric field parallel ($\mathbf{E}_{\parallel}$) and perpendicular ($\mathbf{E}_{\perp}$) to the c axis are shown in Fig. 2, with ω ranging from 0.01 to 23 eV. The two spectra are quite similar, in particular in the FIR where they tend to coincide.

The low-energy region is characterized by very high values of R, which starts from ~99% at 0.01 eV. By increasing the energy, R rapidly decreases, reaching a minimum at 0.54 and 0.51 eV for $\mathbf{E}_{\parallel}$ and $\mathbf{E}_{\perp}$, respectively. This cutoff in R looks strongly like the minimum at the free-electron plasma frequency ω_p of the metal reflectivity, which in the ideal case marks the transition from the intraband to the interband regime. At higher energies R rises again, indicating the occurrence of interband transitions, and has values between 0.5 and 0.6 up to 8 eV. Above 8 eV, both spectra show a decreasing tail up to about 12 eV, and then a lower broad band centered around 15–16 eV.

We analyzed the polarized R spectra out of the ellipsometric range by KK analysis. We recall that the reflection coefficient $\tilde{r}(\omega) = r(\omega)e^{i\theta(\omega)}$ is related to $R(\omega)$ by $R(\omega) = \tilde{r}(\omega)[\tilde{r}(\omega)]^*$ and that the phase dispersion $\theta(\omega)$, for normal incidence, is[19]

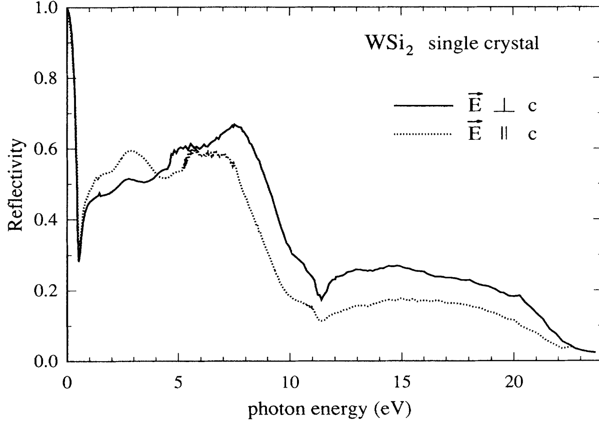

FIG. 2. Near-normal polarized reflectivity of WSi_2 single crystal between 0.01 and 23 eV. The electric field **E** is perpendicular (full line) or parallel (dotted line) to the c axis.

$$\theta(\omega) = \frac{\omega}{\pi}\int_0^{\infty} [\ln R(\omega') - \ln R(\omega)](\omega^2 - \omega'^2)^{-1} d\omega'. \quad (8)$$

The complex refractive index $\tilde{n} = n + ik$ is connected to r and θ by

$$n = (1 - r^2)/(1 + r^2 - 2r\cos\theta), \quad (9)$$

$$k = 2r\sin\theta/(1 + r^2 - 2r\cos\theta). \quad (10)$$

The integrals involved in the numerical treatment require the knowledge of R over a very large photon energy range, in principle from 0 to ∞. This is not possible in practice, and therefore extrapolation becomes necessary. In our case, it should be noticed that (i) at low energy R saturates toward 1; (ii) our spectra are extended up to 23 eV, where the reflectivity tends to decrese rapidly to zero; and (iii) we know directly the complex refractive index from 1.4 to 5 eV by ellipsometry. Therefore we extrapolated the reflectivity R beyond the highest experimental energy ω_0 with a tail $R(\omega) = R(\omega_0)(\omega_0/\omega)^s$. The s value was determined so that the n and k values from KK in the spectral range covered by the ellipsometer reproduce almost exactly the ellipsometric data (the largest discrepancy is of 4%). For both polarizations we obtained $s \approx 2.5$.

The resulting spectra of the complex refractive indexes $\tilde{n}_{\perp}$ and $\tilde{n}_{\parallel}$ are shown in Figs. 3(a) and 3(b), respectively. In the low-energy region their behavior is typical of a metal, starting from very high values (with $k > n$) and rapidly decreasing. For an ideal free-electron metal, at the plasma frequency $n = k \sim 0$. In our real case, the minima in R near 0.5 eV appear in $\tilde{n}$ as crossing points between n and k. We note that there is an energy range in which $k_{\parallel}$ and $k_{\perp}$ are somewhat low, so that the absorption coefficient $\alpha = 4\pi k/\lambda$ is low too. This region lies between the infrared metal-like and the visible strongly absorbing region and, as it will be shown below, it determines a transparency window in the optical response of WSi_2 thin films.

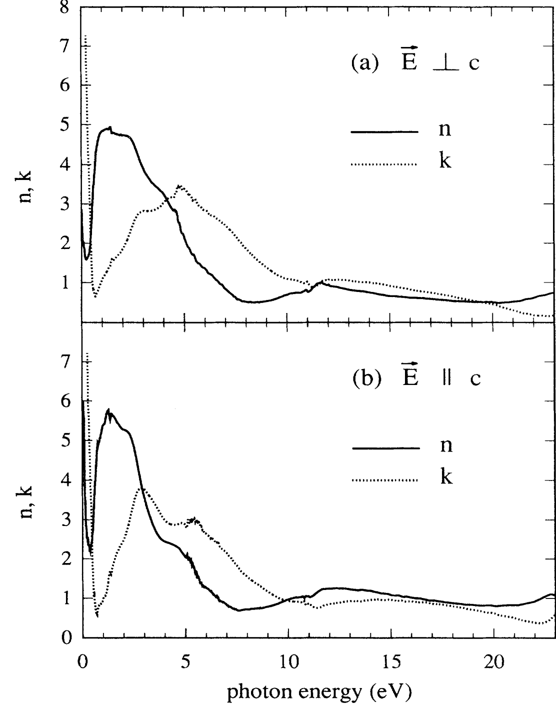

FIG. 3. Real part n (full line) and imaginary part k (dotted line) of the complex refractive index of WSi_2 single crystal. (a) **E** perpendicular to the c axis; (b) **E** parallel to c axis.

We also calculated the complex dielectric function $\tilde{\epsilon}= \tilde{n}^2$. As to the interband region of the dielectric response, which will be discussed in more detail below, we note that the peaks and the shoulders in our spectra of ϵ_2 agree with the ellipsometric results of Ref. 6. As the intraband optical properties are concerned, we analyzed the low-energy response in order to extract the free-electron plasma frequency ω_p and the electronic scattering time τ (or the related damping parameter $\gamma = 1/\tau$). They enter in the Drude dielectric function $\tilde{\epsilon}_{\text{intra}}$ by the equation

$$\tilde{\epsilon}(\omega)|_{\text{intra}} = \epsilon_{\infty} - \frac{\omega_p^2}{\omega(\omega + i\gamma)}, \quad (11)$$

where ϵ_{∞} is the high-frequency dielectric constant. We determined the plasma frequency values from the slope of $1/|\epsilon_1|$ vs ω^2. The values of γ were obtained from the value of the function $\omega\epsilon_2/\epsilon_1$ at the lowest energies, where, according to the Drude limit, it is constant. We obtained $\omega_{p\perp}$=1.7 eV and $\omega_{p\parallel}$=1.8 eV for $\mathbf{E} \perp \vec{c}$ and $\mathbf{E} \parallel \vec{c}$, respectively. The damping parameters are $\gamma_{\perp}$=0.02 eV and $\gamma_{\parallel}$=0.018 eV. The resistivities at zero frequency, calculated as $\rho_{dc} = 4\pi\gamma/\omega_p^2$, result in 10.5 $\mu\Omega$ cm and 9.5 $\mu\Omega$ cm for $\mathbf{E} \perp \vec{c}$ and $\mathbf{E} \parallel \vec{c}$, in very good agreement with those measured by electrical transport in Ref. 5.

B. Optical response of WSi_2 polycrystalline films

The reflectance was measured on silicide films of different thicknesses. The spectra from 0.01 to 3 eV, relative

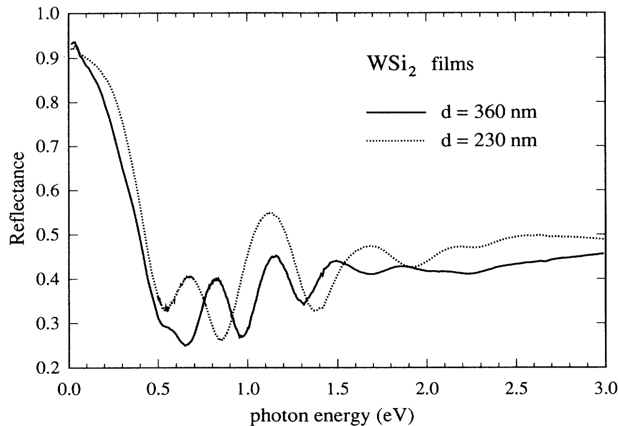

FIG. 4. Reflectance of WSi_2 thin films with different thicknesses d (full line: d=360 nm; dotted line: d=230 nm) in the energy region from 0.01 to 3 eV. Interference fringes appear above 0.5 eV.

to two representative thicknesses (230 and 360 nm), are presented in Fig. 4. Below 0.5 eV all the spectra have the same shape as for the single crystal, but R values are slightly lower in the FIR. Between 0.5 and 3 eV the new striking feature is the presence of optical interference fringes, whose spacing decreases as the film thickness increases. This gives direct evidence that WSi_2 is transparent (or partially transparent) in this spectral region. Finally, for energies higher than 3 eV the reflectance values (not shown in the figure) of silicides with different thicknesses tend to coincide.

We note that, due to the multilayer ($WSi_2/SiO_2/Si$) structure of the samples, we could not determine n and k directly from the experimental data in the interference region. It was therefore necessary to analyze carefully the contributions of the different interfaces to the multireflection process. First, we tried to solve numerically the equations in n and k giving the reflectance for two different WSi_2 thicknesses. A simple method to obtain the reflectance of a multilayer system is the "matrix method,"[20] which states a recurrence relation between the incident electric field and that reflected (transmitted) by a system of N films. Considering the appropriate reflection (transmission) complex Fresnel coefficients $\tilde{r}_m$ ($\tilde{t}_m$) at the mth interface, the problem is solved by calculating a 2×2 complex matrix which results from the product of (N+1) matrices $\tilde{C}_m$, with

$$\tilde{C}_m = \begin{pmatrix} e^{i\tilde{\delta}_{m-1}} & \tilde{r}_m e^{i\tilde{\delta}_{m-1}} \\ \tilde{r}_m e^{-i\tilde{\delta}_{m-1}} & e^{-i\tilde{\delta}_{m-1}} \end{pmatrix}. \quad (12)$$

Here $\tilde{\delta}_{m-1} = 2\pi d_{m-1}\tilde{n}_{m-1}/\lambda$ is the complex phase variation due to the path through the film with thickness d_{m-1}; $\tilde{n}_{m-1}$ is the complex refractive index of the $(m-1)$th layer, and λ is the wavelength in the air. Writing the matrix product as

$$(\tilde{C}_1)(\tilde{C}_2)\cdots(\tilde{C}_{N+1}) = \begin{pmatrix} \tilde{a} & \tilde{b} \\ \tilde{c} & \tilde{d} \end{pmatrix} \quad (13)$$

the reflectance of the multilayer is

$$R = \frac{\tilde{c}\tilde{c}^*}{\tilde{a}\tilde{a}^*}. \quad (14)$$

Therefore, R can be calculated if the N thicknesses and the optical functions of each layer are known.

Since the samples used for the R measurements were nonbacklapped, the interface Si/air was rough enough to scatter in all directions light coming from the WSi_2/SiO_2 system, so that we considered the Si film as an infinite substrate. Moreover, we know both the thickness of each layer from RBS and the optical functions of amorphous SiO_2 and crystalline Si from the literature.[21,22]

The equations $R(n,k,d_i) = R_{\rm expt}(d_i)$, where d_i is the silicide thickness and $R_{\rm expt}$ is the measured reflectance, cannot be solved analytically. We expanded R to the first order in n and k, and we obtained a system of two linear equations, using two different thicknesses. Then, the system solutions were found by an iterative method using the values of n and k estimated by a small number of contour graphs[23] as tentative initial values.

Nevertheless, the numerical method had some troubles. In fact, it is based on an ideal geometrical and structural representation of the multilayer: the interfaces are considered sharp, flat, and parallel, and each layer is assumed homogeneous, with a well-defined complex refractive index. These assumptions are relaxed in the case of real samples, where structural imperfections, such as non-planarity of the interfaces, and transition regions of not-well-defined composition become important. As a consequence the numerical treatment can produce some results with no physical meaning and generate some anomalous dispersions in n and k.

Therefore, we preferred to perform a best fit of the measured reflectances. In the fitting procedure we required that (i) the nonphysical singularities mentioned above were rejected and (ii) n and k satisfied the Kramers-Kronig relations. We also checked the influence of the silicide and the SiO_2 thickness values on the interference spacings. We found that the thicknesses which reproduce the experimental fringes well were in agreement, within the experimental uncertainty, with those measured by RBS.

In Fig. 5 we present the resulting optical functions which best fit $R_{\rm expt}$; the curves between 3 and 5 eV (absorption region) were directly obtained by ellipsometry, because in this spectral region the WSi_2 film can be considered as a bulk. The optical functions n and k rapidly decrease from the high values in the far-infrared region, showing a typical metallic behavior. Near 0.5 eV n starts to increase. However, in this energy region the extinction coefficient k shows a plateau with values sufficiently low to permit a relevant percentage of the incident light to traverse the silicide films, to incide on the silicide/SiO_2 interface, and then to induce multiple internal reflections. For energies higher than 2 eV k increases reaching the value of 2.6 at 3 eV. WSi_2 becomes more and more absorbing, so that the interference phenomenon disappears in the thinner film too.

On the basis of our findings, it appears that the determination of the thickness of SiO_2 layers grown on WSi_2—a request of great technological interest—may

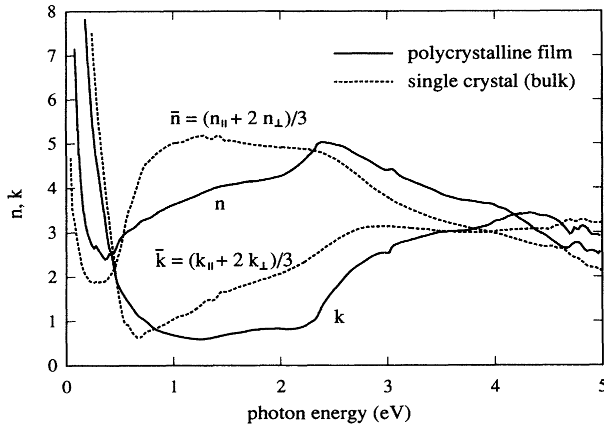

FIG. 5. Complex refractive index $\tilde{n} = n + ik$ of WSi_2 polycrystalline film (full line). The curves are compared with $\overline{n} = (n_{\parallel} + 2n_{\perp})/3$ and $\overline{k} = (k_{\parallel} + 2k_{\perp})/3$ (dashed lines), calculated from the polarized complex refractive indexes of the single crystal.

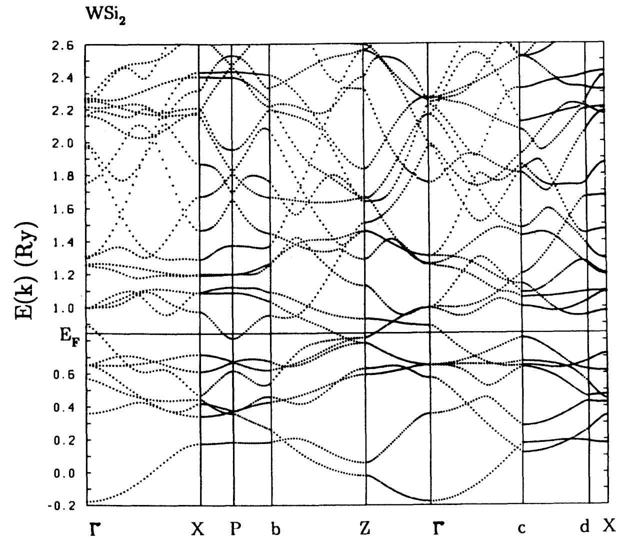

FIG. 6. Self-consistent energy band structure of WSi_2 along some symmetry directions.

create some problems if it is made with a He-Ne standard ellipsometer at λ=632.8 nm.[24] At this wavelength WSi_2 is partially transparent, so that the SiO_2 thickness can be measured only if one knows the silicide complex refractive index and the optical properties of the substrate accurately.

In Fig. 5 we also show the calculated curves $\overline{n} = (2n_{\perp} + n_{\parallel})/3$ and $\overline{k} = (2k_{\perp} + k_{\parallel})/3$, representing the theoretical response of a polycrystal. The comparison with the film response shows for the latter a blueshift of the absorption edge and, in the the energy region between 0.5 and 2.5 eV, a lowering of the values of n and k with respect to the single crystal. These effects in metal films have been attributed[25] primarily to void fraction, as opposed to scattering by defects or grain boundaries. Systematic measurements on several films as a function of the temperature and the annealing time are in progress in order to investigate the origin of this difference in a better way.

C. Energy bands and density of states

The calculated band structure of WSi_2 shown in Fig. 6 is in a rather good agreement with previous calculations.[9,10] It was found that the Fermi surface of WSi_2 consists of two sheets: a hole surface surrounding the Γ point with ellipsoidal shape, and an electron surface in the neighborhood of Z having a boxlike shape with small "horns." In our calculation we found an additional small Fermi surface pocket around the symmetry point P (Fig. 6).

The total and partial densities of states (DOS's) are presented in Fig. 7. The Fermi level is located in the dip of the DOS curve, so that the state density at the Fermi level is rather small. The low DOS at the Fermi level contributes to stabilizing this crystal structure and it is also partially responsible for the small electronic conductivity.

The s electrons of silicon are located mainly near the valence-band bottom whereas the p states of silicon in the occupied part of the valence band are strongly hybridized with the d states of tungsten. This leads to a very similar shape of the energy distribution of silicon $N_p(E)$ and tungsten $N_d(E)$ and implies chemical bonding between silicon and tungsten. The valence band contains a sharp peak at 0.65 Ry. Above the Fermi level the d states of tungsten are mixed with a small amount of silicon p states. The f states of tungsten and d states of silicon are mainly situated far above the Fermi level. Several large peaks may be seen in the energy interval 0.9–1.3 Ry which has mainly tungsten d character. These peaks are due to the 8th to the 11th energy bands and, as will be shown later, play an important role for the structure of the optical functions of WSi_2.

D. Calculated optical properties and comparison with the experiment

In our theoretical investigation, we first calculated the imaginary part of the dielectric function directly [Eq. (1)]. This can be interpreted in terms of interband transitions. A very large anisotropy of the optical properties of WSi_2 was found from both experiment and theory. Figure 8 shows the calculated $\epsilon_2(\omega)$ of WSi_2 for the two different light polarizations $\mathbf{E}\parallel \vec{c}$ and $\mathbf{E}\perp \vec{c}$. There are eight maxima in $\epsilon_2(\omega)$. All these peaks, except for the first one which appears only in the $\mathbf{E}\perp \vec{c}$ polarization, are formed from the same interband transitions for both polarizations. The difference in intensity for the two polarizations is due to the transition matrix element. We inferred from the analysis of the energy dispersion curves $E(\mathbf{k})$ and the energy distribution of the partial densities of states that the interband transitions below 10 eV are due to the excitations of d electrons of tungsten and p electrons of silicon to the unoccupied states, primarily d

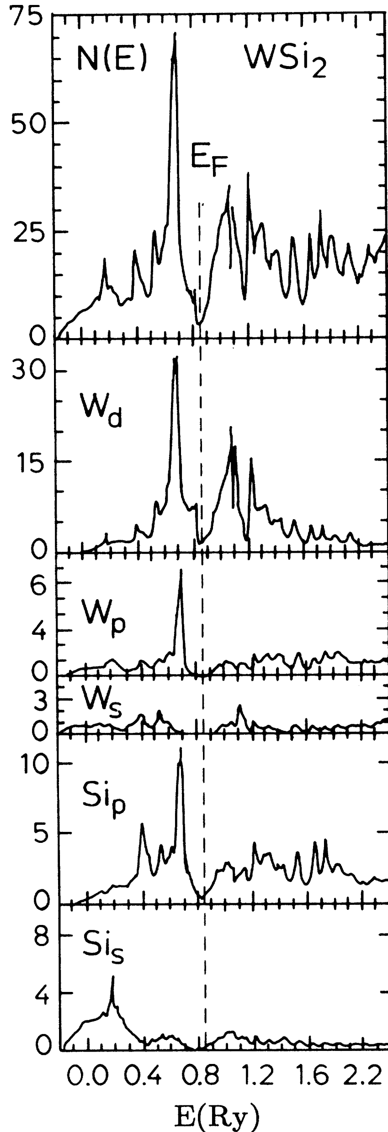

FIG. 7. Self-consistent total density of states $N(E)$ and W s, p, d and Si s and p partial densities of states. Units are number of states/(cell Ry) and number of states/(atom Ry), respectively.

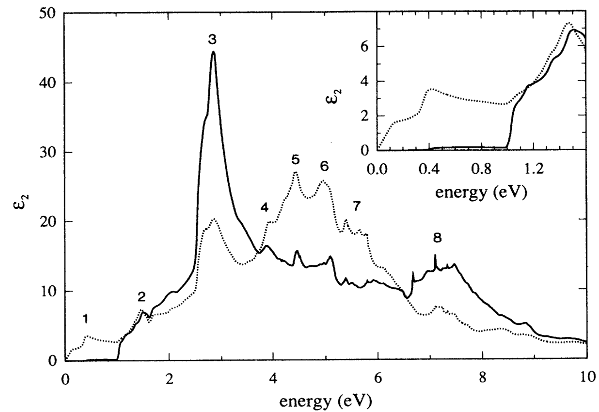

FIG. 8. The calculated imaginary part ϵ_2 of the dielectric function of WSi_2. Full line is for $\mathbf{E} \parallel \vec{c}$ and dotted line is for $\mathbf{E} \perp \vec{c}$.

type, of tungsten which have an admixture of p character. The main contribution to $\epsilon_2(\omega)$ comes from transitions between occupied 5th, 6th, and 7th bands located at 0.5–0.8 Ry and 8th, 9th, 10th, and 11th conduction bands located in the 0.9–1.3 Ry interval. The strong maximum in the $\mathbf{E}\parallel \vec{c}$ polarization at 2.9 eV originates from the superposition of two high intensity partial contributions from the 6,7→8 interband transitions. These transitions take place in an extended part of the $\mathbf{k}$ space including the symmetry points Γ, c, Z, P, the symmetry directions Γ-c, b-a, X-P, and the inner part of the BZ. The same peak can be found in the $\epsilon_2(\omega)$ for the other polarization $\mathbf{E}\perp \vec{c}$. Due to the optical transition matrix element the intensity of transitions 6,7→8 is four times weaker for the $\mathbf{E} \perp \vec{c}$ than for the $\mathbf{E} \parallel \vec{c}$ polarization. $\epsilon_2(\omega)$ for $\mathbf{E}\parallel \vec{c}$ has a threshold at 0.4 eV and is very small up to 1.0 eV in contrast to $\mathbf{E}\perp \vec{c}$, which has a noticeable maximum at 0.4 eV (see Fig. 8). This maximum comes from 7→8 interband transitions in the a-Z symmetry direction where the 7th energy band is very flat. The infrared interband transitions near zero energy (in $\mathbf{E}\perp \vec{c}$) is due to the existence of the doubly degenerate 7th/8th energy band crossing the Fermi level in the Γ-Z symmetry direction. The small structure number two, which has the same size for both polarizations, is formed by the 8→ 9 interband transitions around the Z point. Peak number 4 at 4 eV comes from the 5→8 transitions in the Γ-c direction, where the 5th energy band has a small dispersion. The most intensive 5th maximum in $\mathbf{E}\perp \vec{c}$ polarization at 4.4 eV is formed by transition from the 6th to the 8th energy band in a wide area of $\mathbf{k}$ space including d-c, a-b symmetry directions and in the neighborhood of the Γ and d points. The 6th maximum at 5 eV comes from 6→9 transitions in the vicinity of the a, b, and c points and the a-b symmetry direction. Several peaks numbered 7 around 5.5 eV are formed by 6→9 interband transitions close to the c point, around the a point and the symmetry direction a-b. The 8th peak at 7.2 eV comes from 6,7→11 transitions for both polarizations. These transitions occur around the symmetry points Z, c, and P, and the symmetry directions Γ-c, and Γ-X.

The comparison between the calculated ϵ_2 and the experimental one is shown in detail in Fig. 9.

The calculated values of the plasma frequencies are $\omega_{p\parallel}$=2.53 eV and $\omega_{p\perp}$=2.87 eV, to be compared with those previously extracted by our Drude analysis (1.88 eV and 1.78 eV, respectively). The agreement, within the limits of the theoretical calculation, is good. The anisotropy in the plasma frequency gives rise to the anisotropy of the reflectivity in the infrared region (Fig. 10). For both polarizations the reflectivities fall off very rapidly in the infrared spectral region (this is a direct consequence of the imposition γ=0), but the positions of their minima are different. The minima of

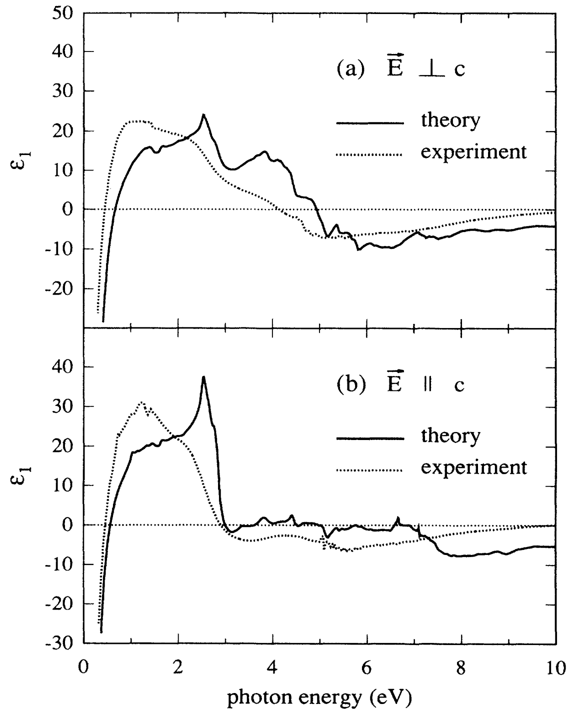

FIG. 9. Comparison between the calculated (full line) and the experimental (dotted line) ϵ_2 curves of WSi_2 single crystal. (a) **E** perpendicular to the c axis; (b) **E** parallel to c axis.

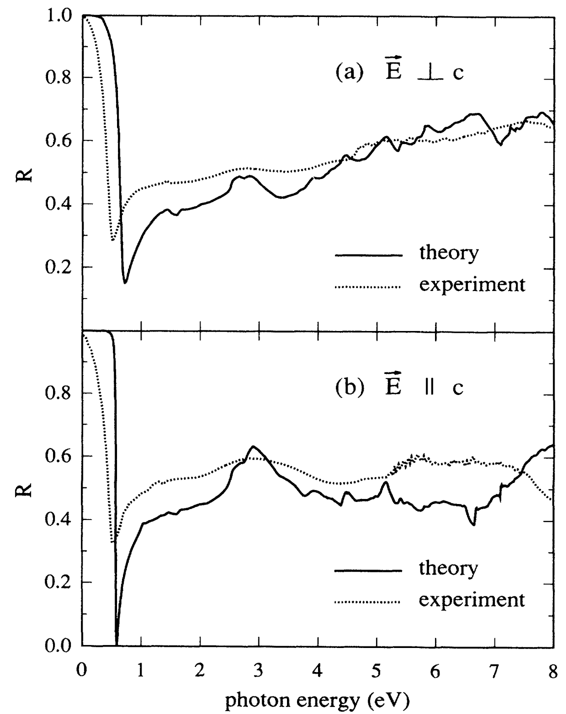

FIG. 10. Comparison between the calculated (full line) and the experimental (dotted line) reflectivity curves of WSi_2 single crystal. (a) **E** perpendicular to the c axis; (b) **E** parallel to c axis.

$R_{\parallel}(\omega)$ and $R_{\perp}(\omega)$ are located at 0.59 and 0.63 eV, respectively. It is interesting to note that the theoretical value of $R_{\mathrm{min},\parallel}(\omega)$ is practically equal to zero, and $R_{\mathrm{min},\perp}(\omega)$ is equal 0.15. In the experiment it is opposite: the minimum in $R_{\perp}(\omega)$ is deeper than in $R_{\parallel}(\omega)$. This discrepancy is caused by the smoothing of the measured spectra due to the finite lifetime effects, lattice imperfections, and distortions. Furthermore, $R_{\parallel}(\omega)$ falls off more rapidly (has a narrower minimum) in comparison with $R_{\perp}(\omega)$.

The theory predicts also a strong anisotropy of $\epsilon_{1\parallel}(\omega)$ and $\epsilon_{1\perp}(\omega)$ (see Fig. 11) which goes through zero at 0.57 and 0.67 eV, respectively. The second sign changes of $\epsilon_{1\parallel}(\omega)$ and $\epsilon_{1\perp}(\omega)$ occur at 3.0 and 4.95 eV and they appear at the same energies as the maxima number 3 and 5 (see Fig. 8) in $\epsilon_{2\parallel}(\omega)$ and $\epsilon_{2\perp}(\omega)$. In this case the change of sign of $\epsilon_{1\parallel}(\omega)$ and $\epsilon_{1\perp}(\omega)$ reflects only the anomalous dispersion of these functions in the region of strong interband absorption. The $\epsilon_{1\parallel}(\omega)$ and $\epsilon_{1\perp}(\omega)$ curves vanish again at 20.6 and 20.3 eV, respectively. Since in this range the imaginary part of the dielectric function is very low, the conditions for a plasma resonance are satisfied. There is a strong resonance maximum at this energy in the calculated electron energy-loss spectra $L(\omega)$ for both polarizations.

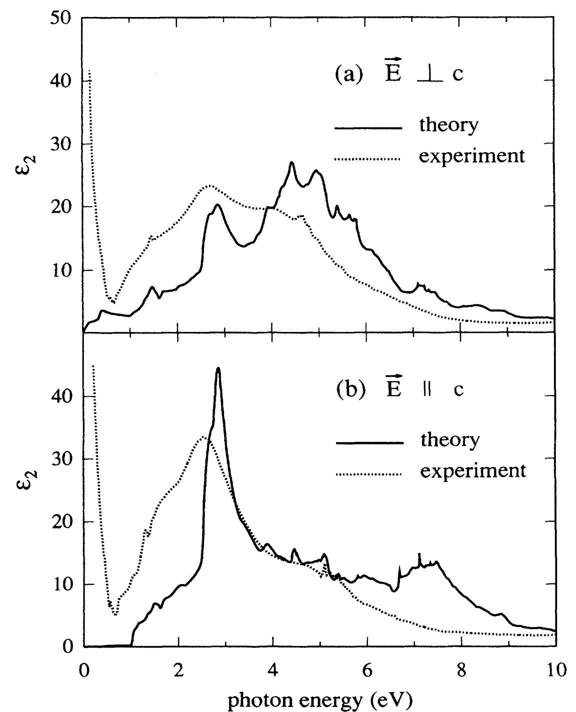

FIG. 11. Comparison between the calculated (full line) and the experimental (dotted line) real part ϵ_1 of the dielectric function of WSi_2 single crystal. (a) **E** perpendicular to the c axis; (b) **E** parallel to c axis.

IV. CONCLUSIONS

The optical characterization of WSi_2 has been carried out on a quite large spectral range with the light polar-

ized along the two different crystallographic directions. From the theoretical point of view, the dielectric functions ϵ_1 and ϵ_2 have been evaluated and compared with the experimental data from 0 up to 10 eV, where good agreement exists.

This excellent agreement between the calculated LDA and the measured optical properties suggests that the nonlocal many-body corrections[26] to LDA are rather small, perhaps, due to the wide energy bands in this system.

At low energies free-carrier (metallic) behavior is expected and observed. The plasma frequency, obtained by inspection of the Drude behavior, is $\omega_{p\perp}=1.7$ eV for the $\mathbf{E} \perp \vec{c}$ polarization and $\omega_{p\|}=1.8$ eV for the $\mathbf{E} \parallel \vec{c}$ polarization. These values agree with the calculated ones, within the intrinsic limits of the theory. The most prominent interband structures, which appear for both polarizations, are located at 1.6, 2.9, and 4 eV, respectively. Furthermore, for energies larger than 0.5 eV and below 3 eV the values of the absorption coefficient remain rather low, permitting the material to become transparent. This effect is enhanced in polycrystalline silicide films, where a blueshift of the absorption edge is also observed.

In the theoretical calculations the observed structures could be assigned to definite interband transitions which are essentially due to the excitations in an extended part of the $\mathbf{k}$ space of d electrons of tungsten and p electrons of silicon to the unoccupied, primarily d type states of tungsten which have an admixture of p character.

ACKNOWLEDGMENTS

This work was partially supported by Progetto Finalizzato "Materiali e Dispositivi per Elettronica a Stato Solido" and by Gruppo Nazionale Struttura della Materia del Consiglio Nazionale delle Ricerche, Italy. The authors acknowledge Professor R. Madar of the Ecole Nationale Supérieure de Physique de Grenoble, who grew and made available the samples and Professor P. Wachter of the Swiss Federal Institute of Technology of Zurich for the permission to use some spectrometers. They are very grateful to Professor Gumlich and to H.Ch. Mertins of the Technische Universität of Berlin, who made it possible and provided assistance in performing the measurements at BESSY. Two of us (V.N.A. and Vl.N.A.) would like to thank the MPI FKF for hospitality during their stay in Stuttgart.

[1] O. Zirinsky, W. Hammer, F. d'Heurle, and J. Baglin, Appl. Phys. Lett. **33**, 76 (1978).
[2] S.P. Murarka, J. Vac. Sci. Technol. **17**, 775 (1980).
[3] F. Nava, K.N. Tu, E. Mazzega, M. Michelini, and G. Queirolo, J. Appl. Phys. **61**, 1085 (1987).
[4] Ch. Krontiras, I. Suni, F.M. d'Heurle, F.K. LeGoues, and R. Joshi, J. Phys. F **17**, 1953 (1987).
[5] F. Nava, E. Mazzega, M. Michelini, O. Laborde, O. Thomas, J.P. Senateur, and R. Madar, J. Appl. Phys. **65**, 1584 (1989).
[6] F. Ferrieu, C. Viguier, A. Cros, A. Humbert, O. Thomas, R. Madar, and J.P. Senateur, Solid State Commun. **62**, 455 (1987).
[7] M. Amiotti, A. Borghesi, G. Guizzetti, F. Nava, and G. Santoro, Europhys. Lett. **14**, 587 (1991).
[8] B.K. Bhattacharyya, D.M. Bylander, and L. Kleinman, Phys. Rev. B **32**, 7973 (1985).
[9] S. Itoh, J. Phys. Condens. Matter **2**, 3747 (1990).
[10] S. Itoh, Mater. Sci. Engineering B **6**, 37 (1990).
[11] U. von Barth, and L. Hedin, J. Phys. C **4**, 2064 (1971).
[12] O. Thomas, Ph.D. thesis, Institut National Polytechnique de Grenoble, 1986.
[13] N.N. Matyushenko, Poroshk. Metall. **1**, 20 (1964).
[14] C.J. Bradley, and A.P. Cracknell, *The Mathematical Theory of Symmetry in Solids* (Clarendon, Oxford, 1972).
[15] O.K. Andersen, Phys. Rev. **12**, 3060 (1975).
[16] H.L. Skriver, *The LMTO Method* (Springer, Berlin, 1984).
[17] O. Jepsen and O.K. Andersen, Solid State Commun. **9**, 1763 (1971).
[18] H. Ehrenreich, and M.H. Cohen, Phys. Rev. **115**, 786 (1959).
[19] F. Stern, in *Solid State Physics*, edited by F. Seitz and D. Turnbull (Academic, New York, 1968), Vol. 15, p. 331.
[20] O.S. Heavens, *Optical Properties of Thin Solid Films* (Butterworths, London, 1955), p. 69.
[21] H.R. Philipp, in *Handbook of Optical Constants of Solids*, edited by E.D. Palik (Academic, Orlando, 1985), p. 749.
[22] D.F. Edwards, in *Handbook of Optical Constants of Solids*, edited by E.D. Palik (Academic, Orlando, 1985), p. 547.
[23] J.E. Nestell, Jr. and R.W. Christy, Appl. Opt. **11**, 643 (1972).
[24] R.D. Frampton, E.A. Irene, and F.M. d'Heurle, J. Appl. Phys. **59**, 978 (1986).
[25] D.E. Aspnes, E. Kinsbron, and D.D. Bacon, Phys. Rev. B **21**, 3290 (1980).
[26] R.W. Godbly, M. Schluter, and L.J. Sham, Phys. Rev. Lett. **56**, 2415 (1986); Phys. Rev. B **36**, 6497 (1987).